DOI: 10.1002/ejic.200600203

Layered Double Hydroxides Containing Intercalated Zinc Sulfide Nanoparticles: Synthesis and Characterization

Guoqing Wu,[a] Lianying Wang,[a] David G. Evans,[a] and Xue Duan*[a]

Keywords: Layered compounds / Intercalations / Zinc complex / Organic–inorganic hybrid composites / ZnS nanoparticles

Nanosized ZnS has been synthesized in the interlayer galleries of Mg–Al layered double hydroxides (LDHs) by a process involving ion exchange of a Mg_2Al-NO_3 LDH precursor with a zinc–citrate complex $\{Na_2[Zn(C_6H_4O_7)]\cdot 3H_2O\}$ followed by reaction between the intercalated $[Zn(C_6H_4O_7)]^{2-}$ anions and H_2S. The materials have been characterized by elemental analysis, powder X-ray diffraction (XRD), transmission electron microscopy, FTIR spectroscopy, MAS ^{13}C NMR spectroscopy, and UV/Vis diffuse reflectance spectroscopy, and structural models have been proposed. The XRD diffraction patterns indicate that the layered structure is maintained and that the basal spacing in the intercalated materials depends on the orientation of the citrate moiety. The results confirm that cubic ZnS (sphalerite) is formed in the interlamellar domain rather than on the external surfaces and is co-intercalated with citrate dianions. The growth of ZnS particles is constrained by the layers of the LDH resulting in a large blue shift in the bandgap compared with the bulk material. The thermal decomposition process of the hybrid material has been characterized by in situ high-temperature powder XRD and thermogravimetry-differential thermal analysis (TG/DTA) coupled with mass spectrometry. The thermal stability of the zinc–citrate complex anions intercalated in LDHs is lower than that in the sodium salt. Thermal treatment below 270 °C leads to a reorientation of the citrate anions in the interlayer galleries associated with a significant interlayer contraction. No obvious changes in the XRD peaks corresponding to ZnS are apparent below 400 °C, indicating that sintering to form larger particles is successfully inhibited by the layered host; at higher temperatures the ZnS is oxidized with evolution of SO_2.

Introduction

In recent years, semiconductor nanocrystals have attracted considerable attention because of their size- and shape-dependent optical and electronic properties as well as their potential for applications in nanodevices. ZnS is one of the most important II–VI semiconductors and has potential applications in numerous areas including optoelectronics,[1] photocatalysis,[2] and thin-film electroluminescent devices.[3] There have been many reports of attempts to control the size and morphology of ZnS including solvothermal routes,[4] thermal evaporation,[5] reverse micelle templates,[6] as well as intercalation in zeolites,[7] and mesoporous silica MCM-41.[8–10] Layered compounds have also been shown to be potential hosts: by virtue of confining the growth of nanoparticles inside the interlamellar galleries, the reaction zone is spatially constrained by the layers,[11–13] giving rise to conditions similar to those in two-dimensional nanoreactors such as Langmuir–Blodgett (LB) films and self-assembled monolayers.[14,15] One great advantage of such methods compared with lithographic fabrication is that regular nanoscale arrays of materials can be obtained with drastically reduced production costs.[16,17]

Layered double hydroxides (LDHs) are a family of lamellar solids that can be represented by the general formula $[M^{II}_{1-x}M^{III}_x(OH)_2]^{x+}A^{n-}_{x/n}\cdot mH_2O$. The structure of this class of compound, based on the stacking of positively charged layers with hydrated anions in the interlamellar domains, allows relatively high mobility of these anions.[18] It is possible to modulate their properties by changing the nature of the M^{II} and M^{III} cations, their molar ratio, and/or the size of the A^{n-} anion.[19,20] One of the most important properties of such compounds is their high anion-exchange capacities. The lamellar structure and the anion-exchange properties of LDHs make them attractive for technological applications such as ion-exchangers, adsorbents, pharmaceutical stabilizers, and precursors of new catalytic materials.[21–23] There have been many examples of LDHs containing intercalated metal complex anions such as permanganate,[24,25] and coordination complexes.[26–30] In the case of metal oxide species, Suib et al.[24] have reported that manganese oxide species (MnO_x) can be prepared in LDH interlayer galleries by ion exchange followed by in situ post-treatment, whilst Lukashin et al.[31] have reported the synthesis of iron oxide nanoparticles with different morphologies and composition using an LDH as the template. However, synthesis of semiconductor nanoparticles using

[a] State Key Laboratory of Chemical Resource Engineering, Beijing University of Chemical Technology,
Box 98, 15 Beisanhuan Dong Lu, Beijing 100029, China
Fax: +86-1064425385
E-mail: duanx@mail.buct.edu.cn

LDHs as the host structure has not been extensively studied. Sato et al.[12,13] have reported that extremely small particles of CdS and CdS–ZnS mixtures less than 0.4 nm in thickness could be prepared by liquid–liquid reactions in the interlayers of LDH and their photocatalytic properties in respect of hydrogen evolution from Na_2S, Na_2SO_3, and/or 2-aminoethanol under irradiation by visible light have been studied. The interlayer distance of their proposed $[Cd(EDTA)]^{2-}$-intercalated LDH precursor is only 0.762 nm however, which is substantially lower than that subsequently reported for $[Ni(EDTA)]^{2-}$-intercalated LDHs.[26,32] Therefore, the $[Cd(EDTA)]^{2-}$ anions in the precursor, and hence presumably also the resulting CdS in the product, are located on the external surfaces of the LDH rather than in the interlayer galleries.

In this work, we report the synthesis of cubic ZnS (sphalerite) nanoparticles by gas–solid reaction in the confined interlayer gallery space of LDHs and the characterization of the resulting hybrid materials. An anionic zinc citrate complex $\{[Zn(Cit)]^{2-}\}$ [Cit = $C_6H_4O_7^{4-}$] is first intercalated into the LDH by ion exchange with a Mg_2Al-NO_3 LDH precursor, giving a material we denote LDH-Zn(Cit). Subsequent reaction with H_2S at atmospheric pressure affords a material, denoted LDH-ZnS-H_2Cit, containing ZnS nanoparticles in the interlayer galleries of the LDH. Subsequent treatment of LDH-ZnS-H_2Cit with aqueous sodium carbonate solution gives a material, denoted LDH-CO_3-ZnS, containing interlayer carbonate anions and ZnS on the external surfaces of the crystallites. This method provides a simple approach for the synthesis of semiconductor particles in layered double hydroxide materials.

Results and Discussion

The preparation of LDH-ZnS-H_2Cit involves four steps: preparation of $Na_2[Zn(Cit)]\cdot 3H_2O$, synthesis of an LDH-nitrate precursor, intercalation of $[Zn(Cit)]^{2-}$ by anion exchange, and, finally, reaction between $[Zn(Cit)]^{2-}$ and H_2S in the interlayer galleries. The coordination chemistry of citrate is rather complex and a variety of mononuclear and polynuclear complexes have been structurally characterized.[33–37] Generally, trianionic $HCit^{3-}$ is the predominant form above pH 5.8, but it is possible to remove the proton from the hydroxy group to give a tetra-anionic Cit^{4-} species at higher pH; the pH required is lowered considerably when the citrate is coordinated to a transition-metal cation. On the basis of elemental analysis (see Exp. Sect.), FTIR spectroscopy, and solid-state NMR spectroscopy (see below), it can be concluded that the tetra-anionic species was present in the zinc complex prepared under the reaction conditions employed in our work. Citrate coordination presumably involves the alkoxy group, the central carboxylate group, and one terminal carboxylate group with the octahedral coordination shell around zinc being completed by three water molecules. This is consistent with the results from both solution and structural studies of related complexes.[38,39]

Elemental Analysis

Elemental compositions of the precursors and intercalated materials are given in the Experimental Section. The Mg/Al molar ratio in LDH-Zn(Cit) (2.00) and LDH-ZnS-H_2Cit (2.02) is essentially the same as that in the LDH-NO_3 precursor (2.03); the value is slightly lower in LDH-HCit (1.87), suggesting that part of the magnesium is leached from the layers during the synthesis of the LDH-HCit. This is commonly observed during ion-exchange reactions with LDHs.[20,21] Elemental analysis confirms that the nitrate anion in the LDH-NO_3 precursor is completely displaced during the exchange reactions with $[Zn(Cit)]^{2-}$ or $[HCit]^{3-}$, as no detectable amounts of nitrogen are present in either material. The data also suggest that the stoichiometry of the zinc citrate complex is unchanged after intercalation, although a small amount of carbonate anion is co-intercalated along with $[Zn(Cit)]^{2-}$. The analytical data for LDH-Zn(Cit) are consistent with the formula $[Mg_{0.69}Al_{0.33}(OH)_2][Zn(C_6H_4O_7)]_{0.16}(CO_3)_{0.01}\cdot 0.58\,H_2O$. In the case of the $[HCit]^{3-}$ intercalate, the data suggest a stoichiometry $[Mg_{0.65}Al_{0.35}(OH)_2](C_6H_5O_7)_{0.11}(CO_3)_{0.01}\cdot 0.57\,H_2O$.

When solid LDH-Zn(Cit) is reacted with gaseous H_2S for 5 min, 20 min, and 1 h, the measured S/Zn molar ratio is 0.34, 0.55, and 0.70 respectively. The deviation of the S/Zn ratio from 1:1 implies that the reaction between Zn^{2+} and H_2S is not fully complete. However, when the reaction time was extended to 8 h, the observed S/Zn molar ratio in the resulting sample (LDH-ZnS-H_2Cit) was 0.96, close to the ideal value of unity. The analytical data for LDH-ZnS-H_2Cit are consistent with the formula $[Mg_{0.67}Al_{0.33}(OH)_2][ZnS]_{0.16}(C_6H_6O_7)_{0.16}(CO_3)_{0.01}\cdot 0.70\,H_2O$.

X-ray Diffraction

The XRD patterns of the LDH materials are shown in Figure 1. The patterns are typical of lamellar materials, with a basal reflection and associated harmonics at low angle 2θ and weaker nonbasal reflections at a higher angle. The reflections for LDHs are generally indexed in a three-layer 3R polytype with rhombohedral symmetry (space group $R\bar{3}m$), based on the structure of the mineral hydrotalcite.[40] In this case, the unit cell c-parameter corresponds to three times the basal spacing $d(003)$ and the value of the unit cell a-parameter is calculated from the position of the $d(110)$ reflection near 60° 2θ. The values of the cell parameters and basal spacing (d_{obs}) in the LDH materials are compared in Table 1. The XRD pattern of LDH-NO_3 shows a basal reflection at 0.867 nm, which is similar to that reported in the literature[41,42] for LDHs with Mg/Al of about 2. Intercalation of $HCit^{3-}$ leads to an increase in basal spacing to 1.15 nm, which is also comparable to the values in the literature.[43] The values of the basal spacing in LDH-Zn(Cit) and LDH-ZnS-H_2Cit are very similar to each other (1.21–1.22 nm) and slightly larger than that in LDH-HCit, which may indicate a different orientation of the citrate moiety within the interlayer galleries. The values of the unit cell a-parameter are very similar for LDH-NO_3,

LDH-Zn(Cit), LDH-ZnS-H_2Cit, and LDH-CO_3-ZnS, with a slightly smaller value being observed for LDH-HCit. The value of *a* corresponds to the average distance between metal ions in the layers and as the Shannon crystal radius of Al^{3+} is smaller than that of Mg^{2+}, a decrease in Mg/Al ratio should lead to a lower value of *a*; the XRD data are therefore consistent with the analytical data described above.

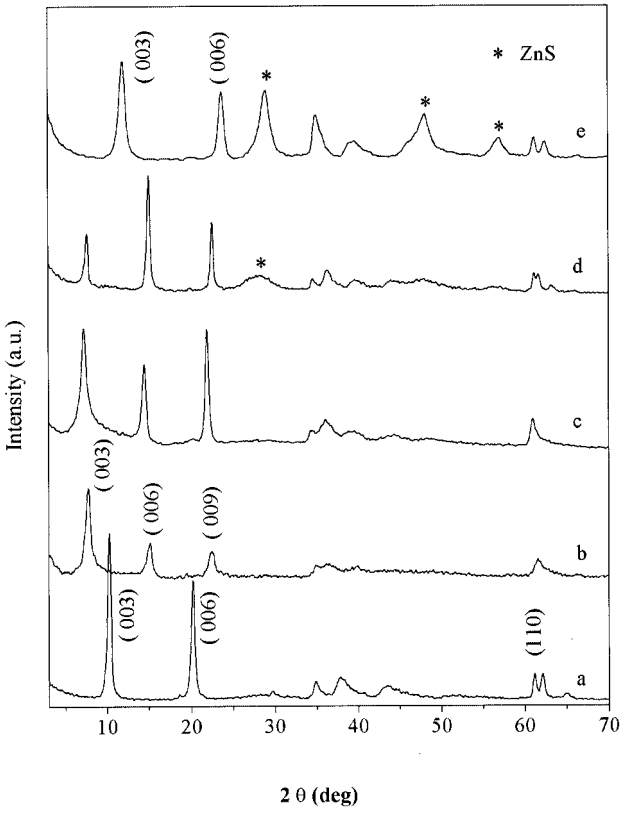

Figure 1. Powder X-ray diffraction patterns of (a) LDH-NO_3, (b) LDH-HCit, (c) LDH-Zn(Cit), (d) LDH-ZnS-H_2Cit, and (e) LDH-CO_3-ZnS.

Table 1. Values of unit cell parameters *a* and *c* and basal spacing *d*(003) for the LDH materials.

Sample	*a* [nm]	*c* [nm]	*d*(003) [nm]
LDH-NO_3	0.303	2.601	0.867
LDH-Zn(Cit)	0.304	3.651	1.217
LDH-ZnS-H_2Cit	0.304	3.633	1.211
LDH-HCit	0.301	3.441	1.147
LDH-CO_3-ZnS	0.303	2.235	0.745

Figure 1 shows the XRD patterns of the LDH-Zn(Cit) precursor and the materials obtained after exposure to H_2S for 8 hours. Although the positions of the (00*l*) (*l* = 3, 6, 9) reflections of LDH-Zn(Cit) and LDH-ZnS-H_2Cit are almost identical, as noted above, there is a significant variation in the relative intensities of the peaks, suggesting that structural changes have occurred within the interlayer galleries. When the interlayer anions in LDHs do not contain any atoms with large scattering power, intensities of the basal (00*l*) reflections are mainly governed by the X-ray intensity scattered by metal cations in the host layers and the intensities generally decrease as *l* increases, as is observed in Figure 1 for LDH-NO_3, LDH-HCit, and LDH-CO_3-ZnS. If the interlayer contains a transition-metal complex anion as the guest, the intensity of the (006) reflection is generally greater than that of (003), which has been attributed to an increased electron density at the midpoint of the interlayers, where the metal is presumed to be located. Reported examples include chromate or vanadate anions intercalated in [Mg–Al] LDHs,[44,45] $[MO_2]^{2-}$ (M = Co, Cu) and $[MOx_3]^{3-}$ (M = Cr, Mn, Ga) (Ox = oxalato) anions in [Zn–Al] and [Mg–Al] LDHs,[29,35] and hexachloro/hydroxoplatinum(IV) anions in [Zn–Al], [Mg–Al], and [Cu–Al] LDHs.[46] It has been reported that 1,1′-ferrocenedicarboxylate and ferrocenecarboxylate anions can be intercalated in [Zn–Al] LDHs giving materials with basal spacings of 1.55 and 2.00 nm respectively.[47] On the basis of modeling studies, these values were interpreted in terms of a monolayer and bilayer of guest species respectively. In the former case, the iron atom is located at the midpoint of the interlayer galleries and, consistent with this picture, the intensity of the (006) reflection is larger than that of (003) and (009). In the bilayer arrangement, alternate iron atoms are shifted along the *c* axis above and below the midpoint of the interlayer galleries, and in this case the intensity of the (009) reflection is larger than that of (006). In the case of LDH-Zn(Cit) (Figure 1, c), the intensity of the (009) reflection is also greater than that of (006), suggesting a similar displacement of the zinc atoms along the *c* axis. On treatment with H_2S, the intensity of the (006) reflection increases, with a concomitant decrease in the relative intensity of the (009) reflection. This indicates that reaction with H_2S involves a change in the one-dimensional electron density distribution alone the *c* axis, which can be ascribed to the migration of the zinc atoms to the midpoint of the interlayer galleries and incorporation of sulfur.

In the case of LDH-ZnS-H_2Cit, a weak broad diffraction peak centered around $2\theta = 28°$ is apparent, which corresponds to the (111) lattice planes of cubic ZnS (sphalerite, JCPDS Card 5-566). The broadness of the peak is indicative of very small nanoparticles; using the Scherrer formula,[48] an average particle diameter of about 2.0 ± 0.2 nm in the direction perpendicular to the (111) lattice planes can be estimated.

It is well known that LDHs have a very strong affinity for carbonate anions. After treatment of LDH-ZnS-H_2Cit with an aqueous solution of sodium carbonate, the resulting solid has a basal spacing of 0.745 nm, which agrees with that reported in the literature for Mg_2Al-CO_3 LDH.[41,49] This indicates that the citrate ions have been displaced by carbonate from the interlayer galleries. Furthermore, the XRD pattern of the resulting material LDH-CO_3-ZnS (Figure 1, e) shows a series of strong and sharp diffraction peaks corresponding to cubic ZnS. This indicates the ZnS nanoparticles have also been liberated from the interlayer galleries by treatment with carbonate anions and, free of the constraint imposed by the layers, grow into larger crys-

tallites on the external surfaces of the LDH. An average particle diameter of about 6.0 nm can be estimated according to the Scherrer formula.[48]

Transmission Electron Microscopy

The transmission electron microscopy (TEM) images of LDH-ZnS-H_2Cit and LDH-CO_3-ZnS are shown in Figure 2. The diameter and shape of the LDH-CO_3-ZnS particles are essentially identical to those of the LDH-ZnS-H_2Cit, which indicates that the extraction of ZnS from the interlamellar galleries does not lead to the destruction of the lamellar structure (see parts a and b in Figure 2). Even at higher magnification (Figure 2, c), there is no obvious indication of the presence of ZnS nanoparticles on the external surfaces of LDH-ZnS-H_2Cit. It is difficult to confirm directly the presence of ZnS in the galleries of the LDHs by the TEM method however; this is probably a result of the weak contrast between the LDH frameworks and the nanosized ZnS, as is the case for ZnS and Fe_2O_3 inside mesoporous hosts.[8,50] In the case of LDH-CO_3-ZnS however, as shown in Figure 2 (d), many ZnS crystallites of about 6.0 nm are observed on the external surfaces. The particle sizes are in agreement with those estimated from the XRD data. The above results show that the small ZnS nanoparticles can only grow in the two-dimensional gallery spaces, where they experience the confinement effect of the layers.

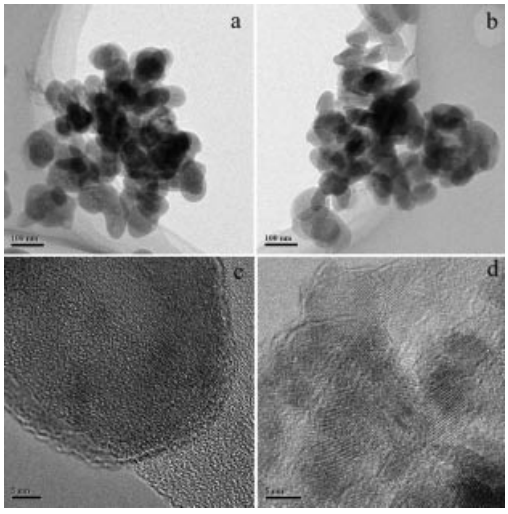

Figure 2. Transmission electron microscopy images of (a) LDH-ZnS-H_2Cit, (b) LDH-CO_3-ZnS at low magnification, (c) LDH-ZnS-H_2Cit, and (d) LDH-CO_3-ZnS at high magnification.

FTIR Spectroscopy

FTIR spectroscopy is very helpful in the study of LDHs, especially those containing interlayer organic anions (or anions with organic moieties), as it is very sensitive to the symmetry of the organic anion and to the interactions of the anion with its environment such as hydrogen bonding and coordinate bonding.[28,39,45,51,52] The FTIR spectra of the Na_2[Zn(Cit)]·3H_2O and Mg_2Al-NO_3 LDH precursors together with those of LDH-Zn(Cit) and LDH-ZnS-H_2Cit are illustrated in Figure 3. For the LDH nitrate precursor (Figure 3, a), the intense and broad absorption band centered at 3445 cm^{-1} corresponds to the stretching vibrations of the hydroxy groups of both the layer hydroxide moieties and interlayer water. The broadening of this band is due to hydrogen-bond formation.[53] The band close to 1640 cm^{-1} corresponds to the deformation mode (δH_2O) of water molecules. The absorption peaks at 1384 and 839 cm^{-1} are usually assigned to the v_3 and v_2 vibration modes, respectively, of NO_3^- with D_{3h} symmetry[42,46] whilst bands around 447 and 675 cm^{-1} are due to Al–O and Mg–O lattice vibrations respectively.[23] The slight broadening of the 1384 cm^{-1} peak and the relatively low wavenumber for the v_2 mode (at 827 cm^{-1}) are indicative of an interaction of NO_3^- anions with their surroundings,[54] namely with intercalated water, hydroxy groups, and metal cations in the brucite-type layers.

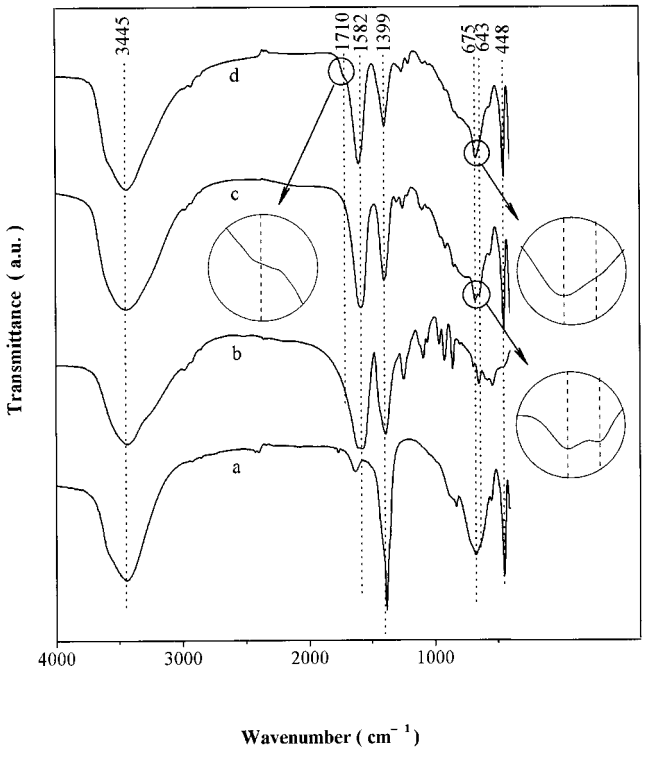

Figure 3. FTIR spectra of (a) LDH-NO_3, (b) Na_2[Zn(Cit)]·3H_2O, (c) LDH-Zn(Cit), and (d) LDH-ZnS-H_2Cit.

The FTIR spectra of the Na_2[Zn(Cit)]·3H_2O precursor (Figure 3, b) exhibits strong characteristic absorptions of the carboxylate group of the citrate ligands in the asymmetric and symmetric vibration regions. Specifically, v_{as}(COO) vibrations appear at 1604 (shoulder) and 1576 cm^{-1} and v_s(COO) vibrations are observed at 1436 (shoulder) and 1393 cm^{-1}. These assignments are in good agreement with those in K_4[MoO_3(Cit)]·3H_2O,[39] which has been structurally characterized and shown to have the same citrate coordination geometry about the metal as that proposed above for Na_2[Zn(Cit)]·3H_2O. The asymmetric v_{as}(COO) and

symmetric ν_s(COO) stretching modes in the complexes are shifted to lower frequencies compared to those of free citrate, denoting the changes in the environment of the ligand upon complexation to metals. The wavenumber difference $\Delta\nu = \nu_{as} - \nu_s$ gives information about the coordination environment of the carboxylate group.[51,55] The value of $\Delta\nu$ for $Na_2[Zn(Cit)]\cdot 3H_2O$ is 183 cm^{-1}, indicating that the carboxylate groups are either free or coordinated to the metal in a monodentate fashion, rather than in bridging or bidentate modes. This is consistent with the structure proposed above for $Na_2[Zn(Cit)]\cdot 3H_2O$.

After exchange of $Mg_2Al\text{-}NO_3$ LDH with $Na_2[Zn(Cit)]\cdot 3H_2O$, the ν_3 vibration of NO_3^- disappears, and the asymmetric ν_{as}(COO) and symmetric ν_s(COO) stretching modes of the carboxylate groups, at 1582 and 1399 cm^{-1} respectively, appear (Figure 3, c). The value of $\Delta\nu$ for LDH-Zn(Cit) (189 cm^{-1}) is similar to that in $Na_2[Zn(Cit)]\cdot 3H_2O$, indicating that the coordination mode of the carboxylate groups is unchanged after intercalation. The slight difference in the value of $\Delta\nu$ may be a reflection of the different intermolecular hydrogen-bonding environments experienced by the anion in the sodium salt and in the interlayer galleries of the LDH.[55–57]

After LDH-Zn(Cit) is exposed to H_2S, the IR spectrum of the resulting material shows a number of changes. The asymmetric ν_{as}(COO) stretching mode shows a shift to 1596 cm^{-1}, comparable to the value for LDH-HCit (1593 cm^{-1}, spectrum not shown). Furthermore, the band at 643 cm^{-1} (see inset of part c in Figure 3) due to the Zn–O vibration mode[23,47] is no longer detected, and an additional IR absorption band at around 1710 cm^{-1}, assigned to the free COOH vibration mode,[34,58,59] appears (see part d in Figure 3, inset), suggesting that (at least) one of the carboxylate groups has been protonated. In $K_4[(MoO_2)_2O(HCit)_2]\cdot 4H_2O$, where the central carboxylate group is protonated, the free COOH vibration mode is observed[39] at around 1715 cm^{-1}. These data all indicate that reaction of intercalated $[Zn(Cit)]^{2-}$ with H_2S leads to cleavage of the Zn–O coordinate bonds in the complex, consistent with the formation of ZnS in the interlayers, according to Equations (1) and (2).

$$H_2S\ (gas) + H_2O\ (interlayer\ water) \rightarrow H_3O^+ + HS^- \quad (1)$$

$$[Zn(Cit)]^{2-} + HS^- + H_3O^+ \rightarrow ZnS + H_2Cit^{2-} + H_2O \quad (2)$$

Solid-State NMR Spectroscopy

Figure 4 shows the solid-state MAS ^{13}C NMR spectra of $Na_2[Zn(C_6H_4O_7)]\cdot 3H_2O$, LDH-Zn(Cit), and LDH-ZnS-H_2Cit. In the spectrum of $Na_2[Zn(C_6H_4O_7)]\cdot 3H_2O$ there are resonances at δ = 184.4 and 181.4 due to the carboxyl groups, and in addition there are two signals of lower frequency at δ = 76.3 due to the alkoxy carbon and at δ = 47.9 due to the methylene carbons. The close correspondence between the MAS ^{13}C NMR spectra of $Na_2[Zn(C_6H_4O_7)]\cdot 3H_2O$ and LDH-Zn(Cit) indicates that the coordination mode of $[Zn(C_6H_4O_7)]^{2-}$ is preserved in LDH-Zn(Cit). In comparison with LDH-Zn(Cit), the corresponding ^{13}C NMR resonances for LDH-ZnS-H_2Cit are all shifted to high field. In particular, the α-carboxyl carbon and β-carboxyl carbon signals show large shifts of $\Delta\delta$ 7.0 and 6.7 ppm, which is a clear indication[39] of the loss of coordination of carboxyl groups to the zinc(II) cation. MAS ^{13}C NMR spectroscopy is unable to confirm whether the central C–O group of the citrate anion is coordinated to the zinc cation as an alcohol or alkoxide group however. Zhou et al.[39] have reported the solid-state NMR spectra of structurally characterized oxomolybdenum(VI) citrate complexes, concluding that the coordination of a deprotonated alkoxide group to molybdenum is characterized by a downfield shift in the ^{13}C resonance to 82–84 ppm compared with that for KH_3Cit ions (δ =74 ppm). It has been reported however[60,61] that the solid-state NMR spectrum of a structurally characterized gallium citrate complex with a deprotonated alkoxide group coordinated to gallium has a peak at δ = 76 ppm. This latter value is very close to those reported for the chemical shifts (73–75 ppm) of a C–OH group in citrate coordinated to cadmium in the solid-state NMR spectra of structurally characterized Cd^{II} complexes.[62] The small difference in chemical shift $\Delta\delta$ between LDH-Zn(Cit) (δ = 76.6 ppm) and LDH-ZnS-H_2Cit (δ = 74.6 ppm) is consistent with the presence of coordinated citrate in the former and free citrate in the latter, although whether the coordination mode in the former involves (C–O–Zn) or [C–O(H)–Zn] linkages cannot be determined. It is noteworthy that the ^{13}C NMR spectrum of LDH-ZnS-H_2Cit is similar to that of the free anion KH_3Cit {^{13}C NMR (D_2O): δ = 177.6 [$(CO_2)_\alpha$], 174.0 [$(CO_2)_\beta$], 73.6 (≡CO), 43.0 (=CH_2)},[39] which is consistent with the IR data.

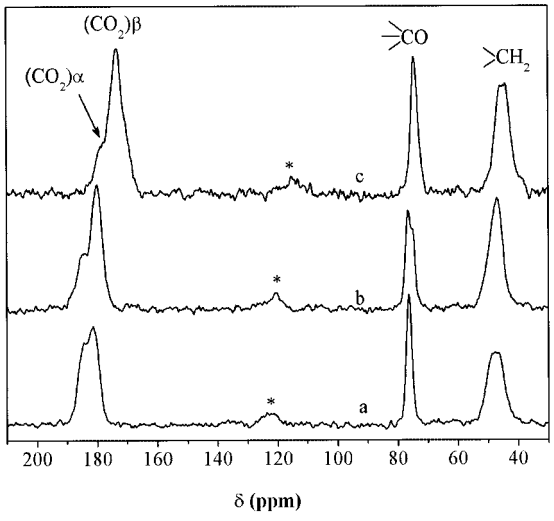

Figure 4. Solid-state ^{13}C MAS NMR spectra of (a) $Na_2[Zn(Cit)]\cdot 3H_2O$, (b) LDH-Zn(Cit), and (c) LDH-ZnS-H_2Cit; spinning sidebands are indicated with an asterisk. α, central carboxylate; β, terminal carboxylate.

Optical Properties of the ZnS Nanoparticles

UV/Vis diffuse reflectance spectroscopy was used to investigate the optical properties of the ZnS nanoparticles. As shown in Figure 5, the LDH-Zn(Cit) precursor has negligible absorption above 250 nm, whereas, in contrast, both LDH-ZnS-H_2Cit and LDH-CO_3-ZnS have significant absorption in the range 250–350 nm, consistent with the presence of ZnS. In comparison with that of bulk ZnS, the absorption onset of LDH-ZnS-H_2Cit shows a blue shift of about 50 nm, whereas the absorption edge of LDH-CO_3-ZnS shows a smaller blue-shift of about 25 nm. The blue shift in UV/Vis spectra, indicating an increase in the bandgap of the material, is associated with a decrease in the particle size, characteristic of the so-called quantum size effects.[63] The smaller blue shift of LDH-CO_3-ZnS relative to that of LDH-ZnS-H_2Cit implies that the former contains larger ZnS particles,[14,64] which is consistent with the XRD data discussed above. The absorption onset for the ZnS nanoparticles is followed by a peak generally referred to as the excitonic peak. The excitonic peak position of the as-prepared ZnS particles in LDH-ZnS-H_2Cit is at 276 nm, corresponding to a bandgap of 4.52 eV, which is some 0.87 eV higher than that in bulk ZnS (3.65 eV).[65] The diameter of the ZnS particles in LDH-ZnS-H_2Cit, as calculated by the Wang equation,[4,63] is about 2.0 nm, which is comparable to the value estimated from XRD (2.0 ± 0.2 nm) as noted above.

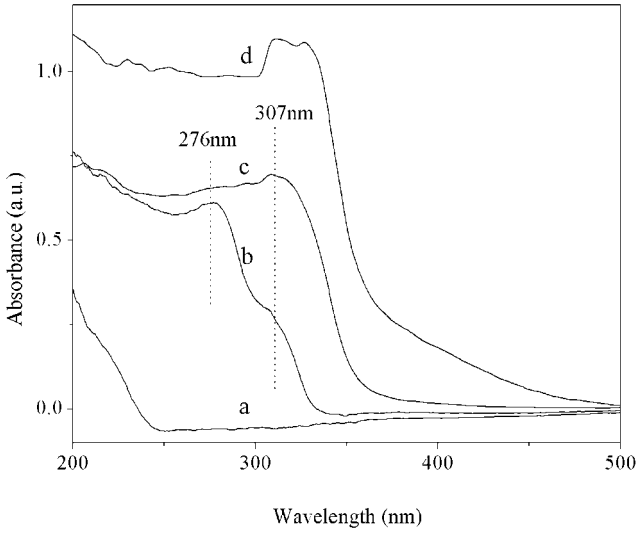

Figure 5. UV absorption spectra of (a) LDH-Zn(Cit), (b) LDH-ZnS-H_2Cit, (c) LDH-CO_3-ZnS, and (d) bulk ZnS (with particles diameter above 1 mm).

The presence of the shoulder (307 nm) on the long wavelength side of the excitonic peak in LDH-ZnS-H_2Cit may be an indication of an anisotropic disk or plate-like morphology of the ZnS particles induced by their confinement in the interlayer galleries. Li et al.[66] have prepared ZnS/octylamine hybrid nanosheets that show two such absorption features, and a similar phenomenon has been observed for CdS nanoparticles in LB films.[14] Alternatively, a high wavelength shoulder may be caused by a large concentration of defect sites (vacancies and interstitial anions).[67,68] Li et al.[69] reported that ZnS nanoparticles with <3 nm average diameter have two absorption features, concluding that the weak shoulder that appeared at 320 nm was caused by sulfur vacancy defects. Similar features have been observed and discussed in the literature for ZnS nanoparticles.[70,71] The spectra of our ZnS nanoparticles thus suggest that the organic component present in the sample may interact with the ZnS particles. The interface induced by the interaction between the ZnS clusters and the organic component in LDH-ZnS-H_2Cit may possess a large number of sulfur vacancy defects, which is consistent with the results of chemical analysis of the S/Zn ratio. Therefore, the optical properties of our ZnS nanoparticles may be similarly influenced by the presence of sulfur vacancy defects.

Structural Model of the Intercalated Materials

All of the experimental results given above indicate that the $[Zn(Cit)]^{2-}$ anion is intercalated in the interlayer galleries and that ZnS nanoparticles are synthesized in situ by reaction with H_2S. If the thickness of the LDH layer (T_{Layer} = 0.21 nm) and the hydrogen-bonding space between the layers and anions ($2L_H$ = 0.27 nm) are subtracted[72] from the observed basal spacing of LDH-Zn(Cit) (see Table 1), the gallery height is calculated to be 0.74 nm. As the estimated length[73] of the $[Zn(Cit)]^{2-}$ anion (with three H_2O molecules) is about 0.79 nm, its long axis is probably oriented perpendicular to the layers (Figure 6, a) with the pendant carboxylate group of adjacent anions hydrogen-bonded to opposite layers. This locates the Zn atoms away from the center of the interlayer galleries, consistent with the relative intensities of the XRD reflections discussed

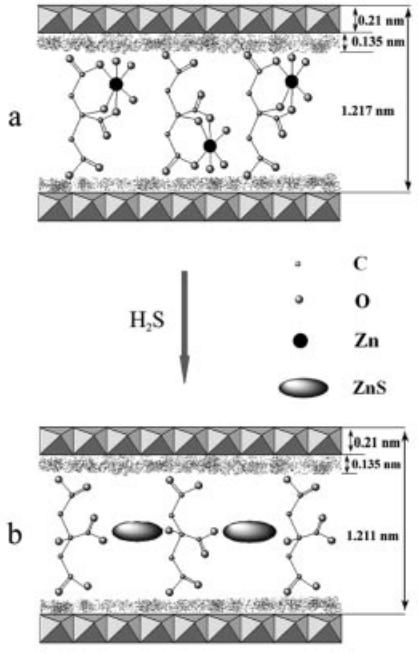

Figure 6. Schematic illustration of the structures of (a) LDH-Zn(Cit) and (b) LDH-ZnS-H_2Cit.

above [$I(009) > I(006)$]. On reaction with H_2S, a change in the one-dimensional electron-density distribution alone the *c* axis occurs, consistent with the formation of ZnS nanoparticles in the center of the interlayer galleries, along with co-intercalated H_2Cit^{2-} anions, as shown schematically in part b of Figure 6.

As discussed above, on the basis of XRD and UV/Vis spectroscopic data, the estimated diameter of the ZnS particles is about 2.0 nm. As the gallery height in LDH-ZnS-H_2Cit is only 0.73 nm, this implies that the particles have a disc- or plate-like morphology. A similar observation has been reported in the literature[14,15,58,74,75] for semiconductor nanoparticles formed in the layers within LB films, where the particles adopt a disc-like morphology as result of the constraints imposed by the two-dimensional nanoreactors.

Thermal Behavior of the Materials

In Situ Variable Temperature XRD Study of LDH-Zn(Cit) and LDH-Zns-H_2Cit

The in situ variable temperature powder X-ray diffraction patterns of LDH-Zn(Cit) and LDH-ZnS-H_2Cit in the temperature range 30–900 °C are shown in Figure 7 and Figure 8 respectively. In each case, as the temperature is increased above ambient, the basal reflections move to higher angles, indicating a contraction in interlayer spacing. The magnitudes of the contraction observed on heating the two samples are very different however. The value of the basal spacing of LDH-Zn(Cit) decreases from 1.217 nm at 30 °C to 1.148 nm at 240 °C. The observed contraction of 0.069 nm can be interpreted in terms of the destruction of the hydrogen-bonding space as a result of removal of interlayer water molecules and the loss of coordinated water molecules from the complex anion (TG measurements on the $Na_2[Zn(C_6H_4O_7)]\cdot 3H_2O$ precursor show that it becomes completely dehydrated below 150 °C). It is worth mentioning that the inversion of intensity between the (006) peak and (009) peak in LDH-Zn(Cit) disappears on heating from 30 °C to 150 °C. This probably results from a disorder in the arrangement of the guests associated with the loss of water molecules from the hydrogen-bonded framework in the interlayer galleries, as water molecules play an important role in preserving interlayer order.[28,41] On further heating above 270 °C, the layer structure collapses completely, indicative of decomposition of the $[Zn(Cit)]^{2-}$ complex and dehydroxylation of the layers. At 400 °C, reflections characteristic of a cubic MgO-like phase begin to appear as a result of decomposition of the layers and at 900 °C reflections from a $MgAl_2O_4$ spinel phase and MgO are present, as is generally observed for calcined [Mg–Al] LDHs.[49,76] In addition, peaks that can be assigned to ZnO (JCPDS Card 01-1136), resulting from the decomposition of $[Zn(Cit)]^{2-}$, can be observed.

In comparison with LDH-Zn(Cit), the value of the basal spacing of LDH-ZnS-H_2Cit shows a much larger contraction of about 0.25 nm on heating from ambient temperature

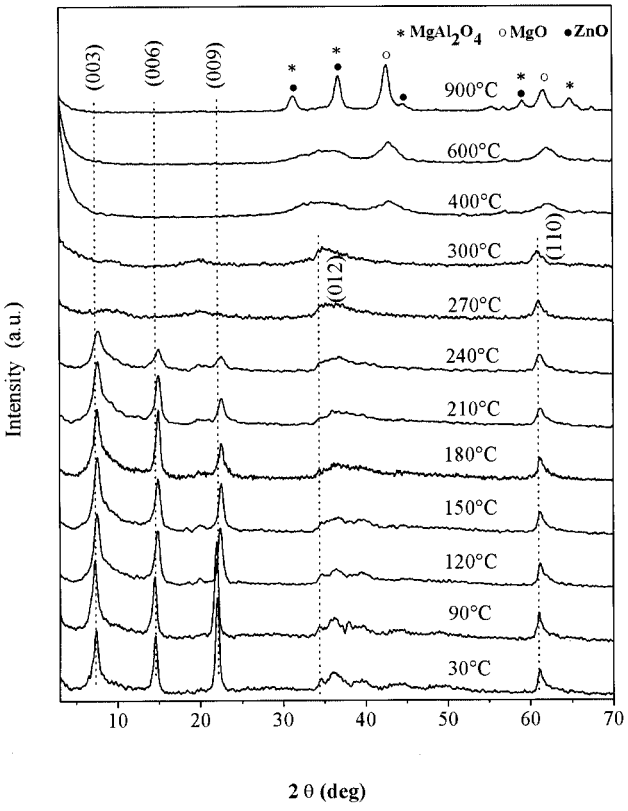

Figure 7. In situ powder X-ray diffraction patterns of LDH-Zn(Cit) in the temperature range 30–900 °C.

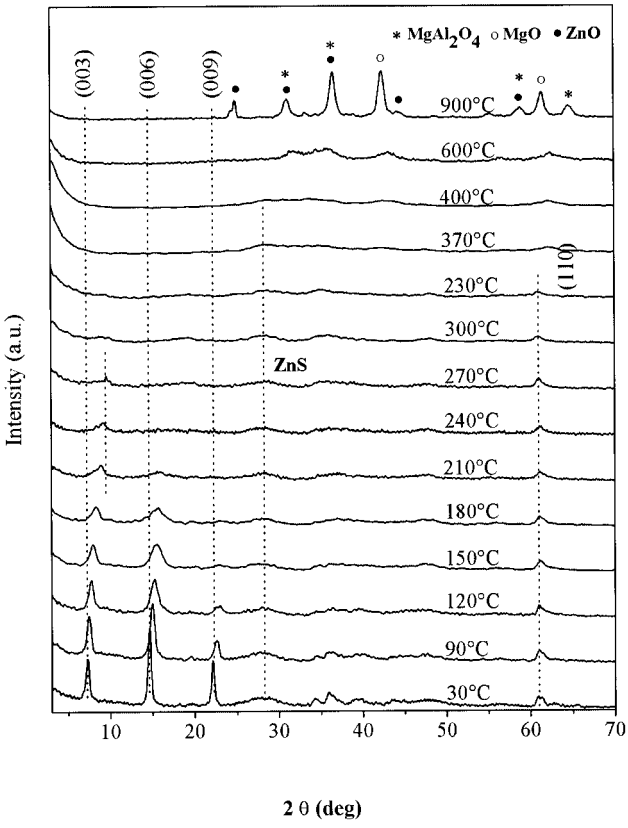

Figure 8. In situ powder X-ray diffraction patterns of LDH-ZnS-H_2Cit in the temperature range 30–900 °C.

to 240 °C, as shown in Figure 8. At 240 °C, evolution of CO_2 is not observed in the MS curve for LDH-ZnS-H_2Cit (see below), implying that decomposition of the intercalated citrate anions does not occur at this temperature. The significant decrease in basal spacing therefore probably results from a reorientation of the free citrate anions from being essentially perpendicular to the layers to being parallel to the layers; a similar phenomenon has been observed for tartrate anions intercalated in LDHs.[77] At 900 °C, peaks attributed to MgO, $MgAl_2O_4$, and ZnO appear, as for LDH-Zn(Cit).

It is noteworthy that the width of the broad diffraction peak centered around $2\theta = 28°$ corresponding to ZnS is essentially unchanged on heating from 30 to 240 °C, implying that there is no growth in particle size with increasing temperature. This provides further evidence that the ZnS nanoparticles are formed in the interlayer galleries rather on the external surfaces of the LDH, as in the latter case considerable sintering would be expected.[8] At 400 °C, the broad diffraction peak of ZnS is no longer observed, which is in agreement with the evolution of SO_2 observed in the MS data for LDH-ZnS-H_2Cit at a similar temperature (see below).

TG/DTA Analysis Coupled with Mass Spectrometry

The results of the thermal analysis of the materials are presented in Figure 9, Figure 10, and Figure 11. Generally, four steps are observed in the thermal evolution of LDHs: desorption of physically adsorbed water, removal of the interlayer structural water, dehydroxylation of the brucite-like sheets, and the decomposition of the interlayer anions, although the first two steps may overlap in the temperature range 30–200 °C and the latter two steps may also overlap at higher temperatures.

For the complex $Na_2[Zn(C_6H_4O_7)]\cdot 3H_2O$ (Figure 9), the thermal decomposition clearly consists of three distinct steps. The first one (30–300 °C, 14.8% mass loss) corresponds to the removal of coordinated water. The sharp mass loss observed in the range 300–400 °C (21.1% mass loss) is due to combustion of the organic ligand, with a corresponding sharp endothermic peak (T_m = 377 °C) in the DTA curve (Figure 9, a). There is a third sharp mass loss step in the range 400–600 °C (10.1% mass loss), with a corresponding strong endothermic peak (T_m = 524 °C) in the DTA curve. Mass spectrometric analysis (Figure 9, b) shows that the first endothermic peak is associated with evolution of both water and carbon dioxide (*m/e* 44, CO_2^+), whilst the second endothermic process involves liberation of CO_2 alone. On this basis $Na_2[Zn(C_6H_4O_7)]\cdot 3H_2O$ decomposes on heating in air by three steps, as in Equations (3), (4), and (5).

$$Na_2[Zn(C_6H_4O_7)]\cdot 3H_2O \rightarrow Na_2Zn(C_6H_4O_7) + 3\ H_2O \quad (3)$$

$$Na_2Zn(C_6H_4O_7) + 9\ O_2 \rightarrow Na_2CO_3 + ZnCO_3 + 2\ H_2O + 4\ CO_2 \quad (4)$$

$$ZnCO_3 \rightarrow ZnO + CO_2 \quad (5)$$

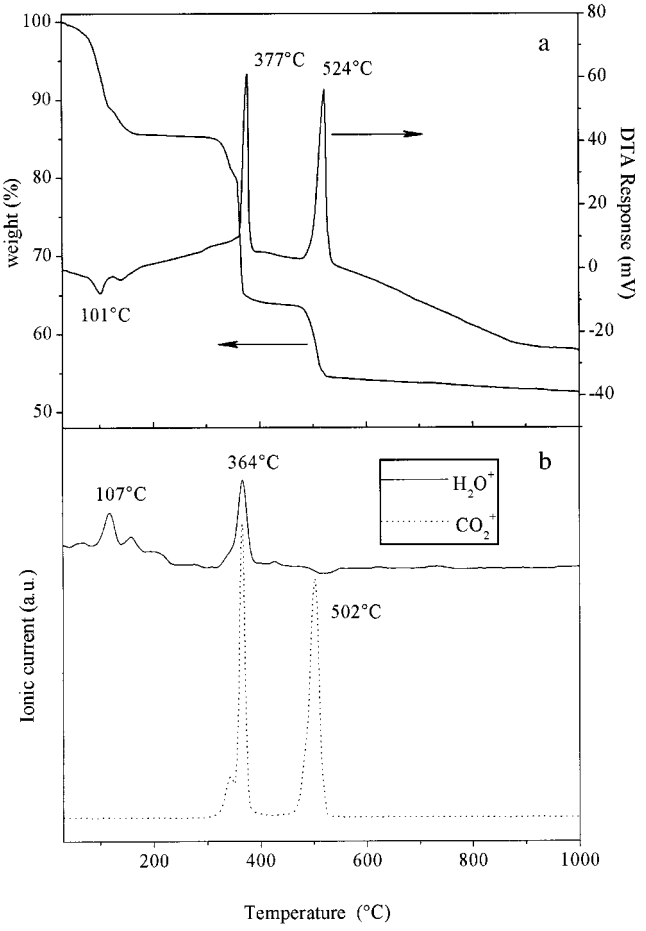

Figure 9. TG/DTA curve (a) and coupled with mass spectrometry curve (b) of $Na_2[Zn(Cit)]\cdot 3H_2O$.

The thermal decomposition of LDH-Zn(Cit) is characterized by three mass loss steps (Figure 10, a). The reduction in mass between 30 and 200 °C (T_m = 120 °C, 9.9% mass loss) is due to loss of surface adsorbed and interlayer water resulting in the decrease in interlayer spacing observed in Figure 7. The latter two mass loss steps overlap to some extent (total weight loss of 37.7%) and are accompanied by exothermic peaks in the DTA at 319 and 417 °C (Figure 10, a). These two exothermic peaks occur some 58 and 107 °C below the temperatures of the corresponding DTA peaks for $Na_2[Zn(C_6H_4O_7)]\cdot 3H_2O$. Typically, the thermal stability of a complex anion intercalated in LDHs is higher than that of the precursor salt.[41] However, the opposite has been reported in the literature,[78,79] as is the case here. Although intercalation of the anion gives rise to a hydrogen-bonding interaction between the pendant terminal COO^- group of the citrate ligand and the layer hydroxy groups, the strongly hydrogen-bonded network of hydrated cations and anions in the precursor salt, clearly demonstrated in the single-crystal structure of $Cu_2(C_6H_4O_7)\cdot 3H_2O$,[33] is lost on intercalation and this may be the origin of the greater thermal stability of the precursor salt. The MS trace (Figure 10, b) shows that both water and carbon dioxide are evolved simultaneously over the entire

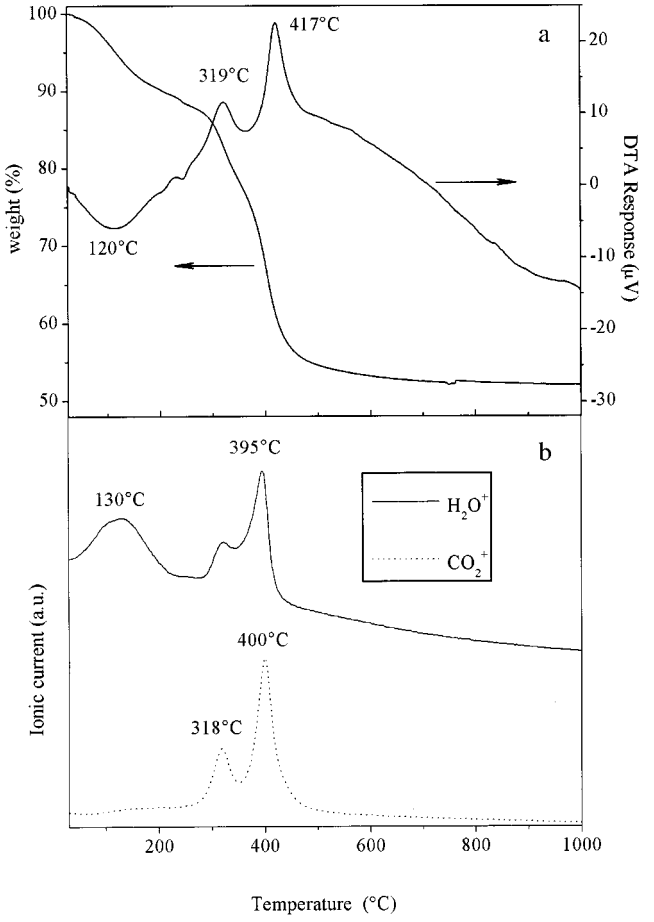

Figure 10. TG/DTA curve (a) and coupled with mass spectrometry curve (b) of LDH-Zn(Cit).

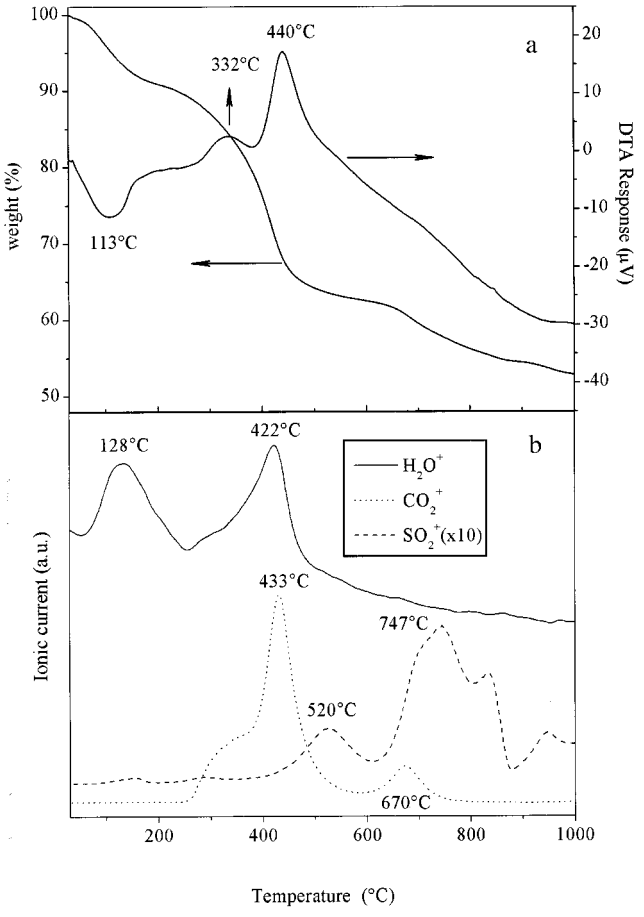

Figure 11. TG/DTA curve (a) and coupled with mass spectrometry curve (b) of LDH-ZnS-H_2Cit.

decomposition range, rather than in discrete steps as seen for $Na_2[Zn(C_6H_4O_7)]\cdot 3H_2O$ (Figure 9, b).

The TG trace for LDH-ZnS-H_2Cit (Figure 11, a) shows also three mass loss events. The first step, corresponding to the removal of surface adsorbed and interlayer water, extends from room temperature to approximately 240 °C (T_m = 113 °C, 10.8% mass loss). The second step (240–540 °C, 25.9% mass loss), with two corresponding exothermic maxima at 332 and 440 °C in the DTA curve, can be assigned to partial decomposition of the citrate ligands and the dehydroxylation of the hydroxide layers. The MS trace (Figure 11, b) shows evolution of both carbon dioxide and water during this process. During the final step (540–950 °C 16.2% mass loss), a gradual weight loss is observed and the MS trace shows that both SO_2 (*m*/*e* 64, SO_2^+) and CO_2 are evolved. The former presumably arises from oxidation of ZnS according to Equation (5) [see Equation (6)]

$$2\ ZnS + 3\ O_2 \rightarrow 2\ ZnO + 2\ SO_2 \quad (6)$$

and is consistent with the absence of the peak assigned to ZnS from the X-ray diffraction patterns recorded above 400 °C. The CO_2 arises from oxidation of residual organic material and as all organic material is lost below 550 °C

Table 2. Results and interpretation of thermogravimetric measurements on precursors and products.

Sample	Temperature range [°C]	Observed step	Experimental mass loss [%]	Calculated[a] mass loss [%]
$Na_2[Zn(Cit)]$	30–300	dehydration	14.8	15.2
	300–600	ligand decomposition	31.2	31.8
LDH-Zn(Cit)	30–200	dehydration	9.9	9.7
	200–700	dehydroxylation + anion decomposition	37.7	38.9
LDH-ZnS-H_2Cit	30–240	dehydration	10.8	9.2
	240–950	dehydroxylation + anion decomposition	42.1	42.9

[a] Mass losses are calculated based on the stoichiometries $Na_2[Zn(C_6H_4O_7)]\cdot 3H_2O$ for $Na_2[Zn(Cit)]$, $[Mg_{0.67}Al_{0.33}(OH)_2][Zn(C_6H_4O_7)]_{0.16}(CO_3)_{0.01}\cdot 0.58H_2O$ for LDH-Zn(Cit) and $[Mg_{0.67}Al_{0.33}(OH)_2][ZnS]_{0.16}(C_6H_6O_7)_{0.16}(CO_3)_{0.01}\cdot 0.70H_2O$ for LDH-ZnS-H_2Cit.

on heating LDH-Zn(Cit), this may indicate that complete combustion of intercalated citrate in LDH-ZnS-H_2Cit is hindered by the presence of co-intercalated ZnS.

The mass losses expected for materials with stoichiometries proposed on the basis of chemical analysis and TGA results are listed in Table 2 and correspond closely to the experimental values.

Conclusions

Cubic sphalerite ZnS nanoparticles can be synthesized by an in situ reaction between a pre-intercalated $[Zn(Cit)]^{2-}$ anion and H_2S in the interlayer galleries of an LDH. The LDH precursor is obtained by an ion-exchange reaction of $Na_2[Zn(C_6H_4O_7)]\cdot 3H_2O$ and a nitrate-containing LDH. The synthesis of the ZnS nanoparticles, involving a gas–solid reaction between the LDH and H_2S, provides a simple approach for the synthesis of such semiconductors in layered hosts. Structural data show that $[Zn(Cit)]^{2-}$ anions are accommodated vertically in the interlayer region as a monolayer with the zinc center in adjacent anions located alternately above and below the midpoint of the interlayer galleries. Reaction with H_2S leads to the formation of co-intercalated ZnS in the interlayer galleries and citrate dianions. The ZnS nanoparticles grow only gradually in the two-dimensional gallery spaces because of the confinement effect of the layers. The material exhibits an excitonic peak at 276 nm corresponding to a bandgap of 4.52 eV, which is some 0.87 eV higher than that in the bulk. The diameter of the ZnS particles (≈ 2 nm), as estimated from XRD and UV/Vis spectroscopic data, is larger than the gallery height of the LDH (0.73 nm), demonstrating that the ZnS nanoparticles have a disc- or plate-like morphology.

Experimental Section

Synthesis: In order to prevent contamination by carbonate ions arising from atmospheric CO_2, all procedures were carried out under constant nitrogen flow using freshly decarbonated, deionized water.

Preparation of $Na_2[Zn(Cit)]\cdot 3H_2O$: A mixture of ZnO (3.91 g, 0.048 mol) and citric acid monohydrate, $C_6H_8O_7\cdot H_2O$ (H_4Cit) (10.09 g, 0.048 mol), was stirred in water (100 mL) until the solids had completely dissolved. The reaction mixture was subsequently stirred overnight at 60 °C. Aqueous sodium hydroxide solution (1.0 M) was added until the pH reached 8.5. After concentration and slow evaporation, a white solid was obtained. The produced solid was redissolved in a water/ethanol mixture, 8:1 (v/v), under mild heating. The derived reaction mixture was allowed to slowly evaporate at room temperature. A few days later, a white crystalline material appeared at the bottom of the flask. The white crystals were isolated by filtration and dried under vacuum. $Na_2[Zn(C_6H_4O_7)]\cdot 3H_2O$ (353.43): calcd. C 20.37, H 2.83, H_2O 15.28, Na 13.02, Zn 18.51; found C 20.58, H 2.56, H_2O 14.87, Na 13.36, Zn 18.93 (H_2O was determined by thermogravimetry as described below). ^{13}C MAS NMR: δ = 47.9 (=CH_2), 76.3 (≡CO), 181.3 [$(CO_2)_\beta$], 184.4 [$(CO_2)_\alpha$] ppm.

LDH-Nitrate Precursor: Mg_2Al-NO_3 LDH was prepared by a co-precipitation method at controlled pH as described in the literature.[80] The resulting white precipitate was collected by centrifugation, washed several times, and stored moist under nitrogen. $[Mg_{0.67}Al_{0.33}(OH)_2](NO_3)_{0.31}(CO_3)_{0.01}\cdot 0.47H_2O$ (87.32): calcd. C 0.15, H 3.36, Al 10.24, H_2O 8.66, Mg 18.39, N 4.99; found C 0.15, H 3.25, Al 10.35, H_2O 9.68, Mg 18.70, N 5.18.

LDH-Zn(Cit): LDH-Zn(Cit) was prepared starting from the as-synthesized LDH-nitrate without drying the solid. The wet LDH-NO_3 (13.75 g, about 10.0 mmol of NO_3^-) was suspended in a solution of $Na_2[Zn(Cit)]\cdot 3H_2O$ (14.14 g, 40.0 mmol) in water (100 mL). The mixture was stirred at room temperature for 8 h in nitrogen. The resulting product was separated by centrifugation, extensively washed, and finally air-dried at 65 °C. $[Mg_{0.67}Al_{0.33}(OH)_2]$-$[Zn(C_6H_4O_7)]_{0.16}(CO_3)_{0.01}\cdot 0.58H_2O$ (109.81): calcd. C 10.28, H 3.49, Al 8.16, H_2O 9.76, Mg 14.60, Zn 9.23; found. C 10.44, H 3.47, Al 8.18, H_2O 9.90, Mg 14.62, Zn 9.22. ^{13}C MAS NMR: δ = 47.1 (=CH_2), 76.6 (≡CO), 180.1 [$(CO_2)_\beta$], 184.9 [$(CO_2)_\alpha$] ppm. For comparison purposes, the $(C_6H_5O_7)^{3-}$-containing LDH (LDH-HCit) was prepared by an analogous procedure. $[Mg_{0.65}Al_{0.35}$-$(OH)_2](C_6H_5O_7)_{0.11}(CO_3)_{0.01}\cdot 0.57H_2O$ (90.62): calcd. C 8.86, H 4.07, Al 10.40, H_2O 10.13, Mg 17.24; found C 8.81, H 3.94, Al 10.32, H_2O 11.30, Mg 17.12.

LDH-ZnS-H_2Cit: Powdered LDH-Zn(Cit) samples were treated with gaseous H_2S for 8 h. The sample is denoted LDH-ZnS-H_2Cit. $[Mg_{0.67}Al_{0.33}(OH)_2][ZnS]_{0.16}(C_6H_6O_7)_{0.16}(CO_3)_{0.01}\cdot 0.70H_2O$ (117.06): calcd. C 9.70, H 3.71, Al 7.63, H_2O 9.65, Mg 13.70, S 4.19, Zn 8.72; found C 9.98, H 3.58, Al 7.26, H_2O 10.79, Mg 13.07, S 3.97, Zn 8.39. ^{13}C MAS NMR: δ = 44.3 (=CH_2), 74.6 (≡CO), 173.4 [$(CO_2)_\beta$], 177.9 [$(CO_2)_\alpha$] ppm.

LDH-CO_3-ZnS: The reaction of LDH-ZnS-H_2Cit with aqueous Na_2CO_3 solution was carried out at 60 °C with a tenfold excess of CO_3^{2-}/Al^{3+} for 2 h. The resulting product was separated by centrifugation, extensively washed, and finally air-dried at 65 °C. The sample is denoted LDH-CO_3-ZnS.

Characterization: Elemental analyses for metals and sulfur were performed by ICP emission spectroscopy using a Shimadzu ICPS-7500 instrument. Carbon, hydrogen, and nitrogen analyses were carried out using an Elementarvario elemental analysis instrument.

The in situ powder X-ray diffraction (in situ XRD) data were recorded with a Shimadzu XRD-6000 powder diffractometer in the temperature range 30–900 °C in air, using Cu-K_α radiation (λ = 0.154 nm) at 40 kV and 30 mA. The samples, as unoriented powders, were step-scanned in steps of 5°/min in the 2θ range from 3 to 70° using a count time of 4 s per step. The rate of temperature increase was 10 °C/min with a holding time of 5 min before each measurement.

FTIR spectra of samples in KBr matrix were recorded with a Bruker Vector 22 spectrophotometer in the range 4000–400 cm^{-1}. UV/Vis diffuse reflectance spectra were recorded at room temperature with a Shimadzu UV-2101PC instrument with $BaSO_4$ powder as the reference.

^{13}C solid-state magic-angle spinning nuclear magnetic resonance (MAS NMR) spectra were recorded with a Bruker AV300 spectrometer operating at a frequency of 75.467 MHz for ^{13}C at a spinning rate of about 4500 Hz with a 5 s pulse delay.

TEM images were obtained with a JEOL 2010 FasTEM at an accelerating voltage of 200 kV. Powder samples were ultrasonically dispersed in ethanol, and the suspension was deposited on a copper grid coated with a holey carbon film.

Thermogravimetric analysis coupled to mass spectrometry was performed using a Perkin–Elmer Diamond TG apparatus linked to a

ThermoStar mass spectrometer by a quartz capillary transfer line heated at 190 °C. The heating rate was 10 °C/min, with an air flow rate of 200 cm^3/min. The TG apparatus was at atmospheric pressure, and the mass spectrometer at a working pressure of 6×10^{-6} Torr. The mass of sample used was 10 mg in each case.

Acknowledgments

This project was supported by the National Nature Science Foundation of China (No. 20401002), Beijing Municipal Education Commission Development Scheme (Project No. JD100100402), and National Basic Research Program (Project No. 2004CB720602).

[1] L. D. Sun, C. H. Liu, C. S. Liao, C. H. Yan, *J. Mater. Chem.* **1999**, *9*, 1655–1657.
[2] H. Fujiwara, H. Hosokawa, K. Murakoshi, Y. Wada, S. Yanagida, *Langmuir* **1998**, *14*, 5154–5159.
[3] P. Calandra, M. Goffredi, L. Turco, *Colloids Surf., A* **1999**, *160*, 9–13.
[4] Y. C. Li, X. H. Li, C. H. Yang, Y. F. Li, *J. Phys. Chem. B* **2004**, *108*, 16002–16011.
[5] Y. Jiang, X. M. Meng, Z. Y. Xie, C. S. Lee, S. T. Lee, *Adv. Mater.* **2003**, *15*, 323–327.
[6] Q. Wu, N. Zheng, Y. Ding, Y. Li, *Inorg. Chem. Commun.* **2002**, *5*, 671–673.
[7] O. Raymond, H. Villavicencio, V. Petranovskii, J. M. Siqueiros, *Mater. Sci. Eng., A* **2003**, *360*, 202–206.
[8] W. H. Zhang, J. L. Shi, H. R. Chen, Z. L. Hua, D. S. Yan, *Chem. Mater.* **2001**, *13*, 648–654.
[9] J. L. Zhang, B. X. Han, Z. S. Hou, Z. M. Liu, J. He, T. Jiang, *Langmuir* **2003**, *19*, 7616–7620.
[10] W. S. Chae, J. H. Yoon, H. N. Yu, D. J. Jang, Y. R. Kim, *J. Phys. Chem. B* **2004**, *108*, 11509–11513.
[11] O. Enea, A. J. Bard, *J. Phys. Chem.* **1986**, *90*, 301–306.
[12] T. Sato, H. Okuyama, T. Endo, M. Shimada, *React. Solids* **1990**, *8*, 63–72.
[13] T. Sato, K. Masaki, T. Yoshioka, A. Okuwaki, *J. Chem. Technol. Biotechnol.* **1993**, *58*, 315–319.
[14] S. W. Guo, L. Konopny, P. B. Ronit, H. Cohen, H. Porteanu, E. Lifshitz, M. Lahav, *J. Am. Chem. Soc.* **1999**, *121*, 9589–9598.
[15] S. W. Guo, P. B. Ronit, T. Arad, G. Hodes, L. Leiserowitz, M. Lahav, *Adv. Mater.* **1998**, *10*, 657–661.
[16] V. I. Srdanov, I. Alxneit, G. D. Stucky, C. M. Reaves, S. P. Den Baars, *J. Phys. Chem. B* **1998**, *102*, 3341–3344.
[17] J. R. Agger, M. W. Anderson, M. E. Pemble, O. Terasaki, Y. Nozue, *J. Phys. Chem. B* **1998**, *102*, 3345–3353.
[18] J. Wang, A. G. Kalinichev, J. E. Amonette, R. J. Kirkpatrick, *Am. Mineral.* **2003**, *88*, 398–409.
[19] J. H. Choy, S. Y. Kwak, Y. J. Jeong, J. S. Park, *Angew. Chem. Int. Ed.* **2000**, *39*, 4041–4045.
[20] A. I. Khan, D. O'Hare, *J. Mater. Chem.* **2002**, *12*, 3191–3198.
[21] A. Vaccari, *Catal. Today* **1998**, *41*, 53–71.
[22] B. Sels, D. De Vos, M. Buntinx, F. Pierard, K. D. Mesmaeker, P. Jacobs, *Nature* **1999**, *400*, 855–857.
[23] V. Rives, in *Layered Double Hydroxides: Present and Future* (Ed.: V. Rives), Nova Science Publishers Inc., New York, **2001**, pp. 139–192.
[24] J. C. Villegas, O. H. Giraldo, K. Laubernds, S. L. Suib, *Inorg. Chem.* **2003**, *42*, 5621–5631.
[25] M. François, J. P. Besse, *J. Solid State Chem.* **2000**, *155*, 332–341.
[26] K. A. Tarasov, D. O'Hare, *Inorg. Chem.* **2003**, *42*, 1919–1927.
[27] M. Kaneyoshi, W. Jones, *J. Mater. Chem.* **1999**, *9*, 805–811.
[28] N. H. Gutmann, L. Spiccia, T. W. Turney, *J. Mater. Chem.* **2000**, *10*, 1219–1224.
[29] P. Beaudot, M. E. De Roy, J. P. Besse, *Chem. Mater.* **2004**, *16*, 935–945.
[30] V. Rives, M. A. Ulibarri, *Coord. Chem. Rev.* **1999**, *181*, 61–120.
[31] M. P. Nikiforov, M. V. Chernysheva, A. A. Eliseev, A. V. Lukashin, Y. D. Tretyakov, Y. V. Maksimov, I. P. Suzdalev, P. Goernert, *Mater. Sci. Eng. B* **2004**, *109*, 226–231.
[32] A. I. Tsyganok, K. Suzuki, S. Hamakawa, K. Takehira, T. Hayakawa, *Chem. Lett.* **2001**, 24–25.
[33] D. Mastropaolo, D. A. Powers, J. A. Potenza, H. J. Schugar, *Inorg. Chem.* **1976**, *15*, 1444–1449.
[34] Z. H. Zhou, S. Y. Hou, H. L. Wan, *Dalton Trans.* **2004**, 1393–1399.
[35] E. R. Still, P. Wikberg, *Inorg. Chim. Acta* **1980**, *46*, 153–155.
[36] Z. H. Zhou, H. L. Wan, K. R. Tsai, S. Z. Hu, *Inorg. Chim. Acta* **1995**, *237*, 193–197.
[37] J. Strouse, S. W. Layten, C. E. Strouse, *J. Am. Chem. Soc.* **1977**, *99*, 562–572.
[38] J. P. Glusker, *Acc. Chem. Res.* **1980**, *13*, 345–352.
[39] Z. H. Zhou, H. L. Wan, K. R. Tsai, *Inorg. Chem.* **2000**, *39*, 59–64.
[40] A. S. Bookin, V. I. Cherkashin, V. Drits, *Clays Clay Miner.* **1993**, *41*, 558–564.
[41] F. Cavani, F. Trifiro, A. Vaccari, *Catal. Today* **1991**, *11*, 173–301.
[42] Z. P. Xu, H. C. Zeng, *J. Phys. Chem. B* **2001**, *105*, 1743–1749.
[43] J. Zhang, F. Zhang, L. L. Ren, D. G. Evans, X. Duan, *Mater. Chem. Phys.* **2004**, *85*, 207–214.
[44] S. Miyata, *Clays Clay Miner.* **1983**, *31*, 305–311.
[45] M. D. Arco, S. Gutiérrez, C. Martín, V. Rives, *Inorg. Chem.* **2003**, *42*, 4232–4240.
[46] P. Beaudot, M. E. De Roy, J. P. Besse, *J. Solid State Chem.* **2001**, *161*, 332–340.
[47] S. Gago, M. Pillinger, T. M. Santos, J. Rocha, I. S. Gonçalves, *Eur. J. Inorg. Chem.* **2004**, 1389–1395.
[48] Y. Wang, N. Herron, *Phys. Rev. B* **1990**, *42*, 7253–7255.
[49] E. Kanezaki, *Solid State Ionics* **1998**, *106*, 279–284.
[50] T. Abe, Y. Tachibana, T. Uematsu, M. Iwamoto, *J. Chem. Soc., Chem. Commun.* **1995**, 1617–1618.
[51] K. Nakamoto, *Infrared and Raman Spectra of Inorganic and Coordination Compounds*, 4th ed., Wiley, New York, **1986**, pp. 231–248.
[52] M. Matzapetakis, C. P. Raptopoulou, A. Tsohos, V. Papaefthymiou, N. Moon, A. Salifoglou, *J. Am. Chem. Soc.* **1998**, *120*, 13266–13267.
[53] F. M. Labajos, V. Rives, M. A. Ulibarri, *J. Mater. Sci.* **1992**, *27*, 1546–1552.
[54] Z. P. Xu, H. C. Zeng, *Chem. Mater.* **1999**, *11*, 67–74.
[55] G. B. Deacon, R. J. Phillips, *Coord. Chem. Rev.* **1980**, *33*, 227–250.
[56] Y. Tomita, K. Ueno, *Bull. Chem. Soc. Jpn.* **1963**, *36*, 1069–1073.
[57] N. Gutmann, B. Müller, H. J. Tiller, *J. Solid State Chem.* **1995**, *119*, 331–338.
[58] L. Konopny, M. Berfeld, R. Popovitz-Biro, I. Weissbuch, L. Leiserowitz, M. Lahav, *Adv. Mater.* **2001**, *13*, 580–584.
[59] X. G. Peng, S. Q. Guan, X. D. Chi, Y. S. Jiang, T. J. Li, *J. Phys. Chem.* **1992**, *96*, 3170–3174.
[60] G. E. Hawkes, P. O'Brien, H. Salacinski, M. Motevalli, I. Abrahams, *Eur. J. Inorg. Chem.* **2001**, 1005–1011.
[61] P. O'Brien, H. Salacinski, M. Motevalli, *J. Am. Chem. Soc.* **1997**, *119*, 12695–12696.
[62] E. T. Kefalas, M. Dakanali, P. Panagiotidis, C. P. Raptopoulou, A. Terzis, T. Mavromoustakos, I. Kyrikou, N. Karligiano, A. Bino, A. Salifoglou, *Inorg. Chem.* **2005**, *44*, 4818–4828.
[63] Y. Wang, A. Suna, W. Mahler, R. Kasowski, *J. Chem. Phys.* **1987**, *87*, 7315–7322.
[64] J. Nanda, S. Sapra, D. D. Sarma, *Chem. Mater.* **2000**, *12*, 1018–1024.
[65] Y. Kayanuma, *Phys. Rev. B* **1988**, *38*, 9797–9805.
[66] J. P. Li, Y. Xu, D. Wu, Y. H. Sun, *Solid State Commun.* **2004**, *130*, 619–622.

[67] S. Wageh, S. L. Zhao, X. R. Xu, *J. Cryst. Growth* **2003**, *255*, 332–337.
[68] J. H. Yu, J. Joo, H. M. Park, S. I. Baik, Y. W. Kim, S. C. Kim, T. Hyeon, *J. Am. Chem. Soc.* **2005**, *127*, 5662–5670.
[69] Y. D. Li, Y. Ding, Y. Zhang, Y. T. Qian, *J. Phys. Chem. Solids* **1999**, *60*, 13–15.
[70] P. Calandra, A. Longo, V. T. Liveri, *J. Phys. Chem. B* **2003**, *107*, 25–30.
[71] N. I. Kovtyukhova, E. V. Buzaneva, C. C. Waraksa, B. R. Martin, T. E. Mallouk, *Chem. Mater.* **2000**, *12*, 383–389.
[72] Q. Yuan, M. Wei, D. G. Evans, X. Duan, *J. Phys. Chem. B* **2004**, *108*, 12381–12387.
[73] E. N. Baker, H. M. Baker, B. F. Anderson, R. D. Reeves, *Inorg. Chim. Acta* **1983**, *78*, 281–285.
[74] S. Vitta, T. H. Metzger, S. S. Major, *J. Chem. Phys.* **1999**, *111*, 11088–11094.
[75] Z. Pan, J. Liu, X. Peng, T. Li, Z. Wu, M. Zhu, *Langmuir* **1996**, *12*, 851–853.
[76] B. Rebours, J.-B. d'Espinose de la Caillerie, O. Clause, *J. Am. Chem. Soc.* **1994**, *116*, 1707–1717.
[77] V. Prévot, C. Forano, J. P. Besse, *Inorg. Chem.* **1998**, *37*, 4293–4301.
[78] C. Li, G. Wang, D. G. Evans, X. Duan, *J. Solid State Chem.* **2004**, *177*, 4569–4575.
[79] V. Prévot, C. Forano, J. P. Besse, *J. Solid State Chem.* **2000**, *153*, 301–309.
[80] S. Miyata, *Clays Clay Miner.* **1975**, *23*, 369–375.

Received: March 7, 2006
Published Online: June 29, 2006

